



## Study of the forward-backward asymmetry of $\Lambda, \bar{\Lambda}$ production in $p\bar{p}$ collisions

The DØ Collaboration  
URL <http://www-d0.fnal.gov>  
(Dated: April 27, 2015)

We study  $\Lambda, \bar{\Lambda}$  production asymmetries in events  $p\bar{p} \rightarrow \Lambda(\bar{\Lambda})X$ ,  $p\bar{p} \rightarrow J/\psi\Lambda(\bar{\Lambda})X$  and  $p\bar{p} \rightarrow \mu^\pm\Lambda(\bar{\Lambda})X$  recorded by the DØ detector at the Fermilab Tevatron collider at  $\sqrt{s} = 1.96$  TeV. We find an excess of  $\Lambda$ 's ( $\bar{\Lambda}$ 's) produced in the proton (antiproton) direction. This forward-backward asymmetry, for  $\Lambda$ 's and  $\bar{\Lambda}$ 's with momenta transverse to the  $p\bar{p}$  beams  $p_T > 2.0$  GeV and rapidity  $0.1 < |y| < 2.2$ , is measured to be  $A_{FB} = 0.0115 \pm 0.0005$  (stat)  $\pm 0.0006$  (syst). We also measure the mean differences in rapidity and longitudinal momentum between the  $\Lambda$ 's and  $\bar{\Lambda}$ 's.

*Preliminary Results, April 2015*

## I. INTRODUCTION

We study  $p\bar{p}$  collisions at a total center of mass energy  $\sqrt{s} = 1.96$  TeV recorded by the DØ detector [1–3] at the Fermilab Tevatron collider. The full data set of  $10.4 \text{ fb}^{-1}$ , collected from 2002 to 2011, is analyzed. Among the particles produced in these collisions are  $\Lambda$ 's and  $\bar{\Lambda}$ 's. In this paper we examine the question of whether the  $\Lambda$  and  $\bar{\Lambda}$  retain some memory of the proton and antiproton direction. If in a  $p\bar{p}$  collision a  $u$  ( $\bar{u}$ ) quark of the proton (antiproton) becomes replaced by an  $s$  ( $\bar{s}$ ) quark, a  $\Lambda$  ( $\bar{\Lambda}$ ) may be produced preferentially in the proton (antiproton) direction. Another cause of forward-backward asymmetry may be interference of leading order and next-to-leading order Feynman diagrams. We choose a coordinate system in which the  $z$  axis is aligned with the proton beam direction (directed 'south' in the DØ detector) and define the rapidity  $y \equiv \ln[(E + p_z)/(E - p_z)]/2$ , where  $p_z$  is the outgoing particle momentum component in the  $z$  direction and  $E$  is its energy in the center of mass frame. We measure four observables: (i) the ‘‘forward-backward asymmetry’’  $A_{FB}$ , i.e. the relative excess of  $\Lambda$ 's ( $\bar{\Lambda}$ 's) in the  $p$  ( $\bar{p}$ ) direction, (ii) the difference of the mean rapidity  $y$  of  $\Lambda$ 's and  $\bar{\Lambda}$ 's:  $\langle y(\Lambda) \rangle - \langle y(\bar{\Lambda}) \rangle$ , (iii) the difference of the mean longitudinal momentum of  $\Lambda$ 's and  $\bar{\Lambda}$ 's:  $\langle p_z(\Lambda) \rangle - \langle p_z(\bar{\Lambda}) \rangle$ , and (iv) the ‘‘north-south’’ asymmetry  $A_{NS}$ , i.e. the relative excess of  $\Lambda$ 's plus  $\bar{\Lambda}$ 's with longitudinal momentum in the  $\bar{p}$  direction (north), with respect to the  $p$  direction (south). The measurement of  $A_{NS}$  is a test of CP violation. The measurements include  $\Lambda$ 's and  $\bar{\Lambda}$ 's from all sources (either directly produced or as decay products of heavier hadrons).

The  $\Lambda$ 's ( $\bar{\Lambda}$ 's) are defined as ‘‘forward’’ if their longitudinal momentum is in the  $p$  ( $\bar{p}$ ) direction. The asymmetries  $A_{FB}$  and  $A_{NS}$  of  $\Lambda, \bar{\Lambda}$  production are defined as

$$\begin{aligned} A_{FB} &\equiv \frac{\sigma_F(\Lambda) - \sigma_B(\Lambda) + \sigma_F(\bar{\Lambda}) - \sigma_B(\bar{\Lambda})}{\sigma_F(\Lambda) + \sigma_B(\Lambda) + \sigma_F(\bar{\Lambda}) + \sigma_B(\bar{\Lambda})}, \\ A_{NS} &\equiv \frac{-\sigma_F(\Lambda) + \sigma_B(\Lambda) + \sigma_F(\bar{\Lambda}) - \sigma_B(\bar{\Lambda})}{\sigma_F(\Lambda) + \sigma_B(\Lambda) + \sigma_F(\bar{\Lambda}) + \sigma_B(\bar{\Lambda})}, \end{aligned} \quad (1)$$

where  $\sigma_F(\Lambda)$  and  $\sigma_B(\Lambda)$  ( $\sigma_F(\bar{\Lambda})$  and  $\sigma_B(\bar{\Lambda})$ ) are the forward and backward cross-sections of  $\Lambda$  ( $\bar{\Lambda}$ ) production.

We observe  $\Lambda$ 's and  $\bar{\Lambda}$ 's through their decays  $\Lambda \rightarrow p\pi^-$  and  $\bar{\Lambda} \rightarrow \bar{p}\pi^+$ . Fitting the invariant mass histograms of  $p\pi^-$  we obtain the numbers  $N_F(\Lambda)$  and  $N_B(\Lambda)$  of reconstructed  $\Lambda$ 's in the ‘‘forward’’ and ‘‘backward’’ categories, respectively. Fitting the invariant mass histograms of  $\bar{p}\pi^+$  we obtain the numbers  $N_F(\bar{\Lambda})$  and  $N_B(\bar{\Lambda})$  of reconstructed  $\bar{\Lambda}$ 's in the ‘‘forward’’ and ‘‘backward’’ categories, respectively. Alternatively, we obtain these numbers by counting  $\Lambda$  and  $\bar{\Lambda}$  candidates in a signal region and subtracting the corresponding counts in two side band regions. These numbers define the raw asymmetries  $A'_{FB}$  and  $A'_{NS}$ :

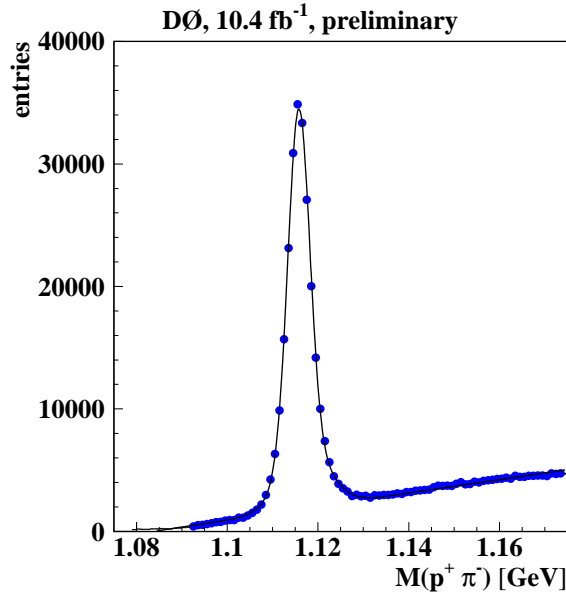
$$\begin{aligned} A'_{FB} &\equiv \frac{N_F(\Lambda) - N_B(\Lambda) + N_F(\bar{\Lambda}) - N_B(\bar{\Lambda})}{N_F(\Lambda) + N_B(\Lambda) + N_F(\bar{\Lambda}) + N_B(\bar{\Lambda})}, \\ A'_{NS} &\equiv \frac{-N_F(\Lambda) + N_B(\Lambda) + N_F(\bar{\Lambda}) - N_B(\bar{\Lambda})}{N_F(\Lambda) + N_B(\Lambda) + N_F(\bar{\Lambda}) + N_B(\bar{\Lambda})}. \end{aligned} \quad (2)$$

The raw asymmetries  $A'_{FB}$  and  $A'_{NS}$  have contributions from the physical processes of the  $p\bar{p}$  collisions ( $A_{FB}$  and  $A_{NS}$  respectively), and from detector effects. The double differences in Eq. (2) help separate detector from physics effects as explained below. The raw asymmetry  $A'_{NS}$  is different from zero if the north half of the DØ detector has a different acceptance times efficiency than the south half of the detector. The initial  $p\bar{p}$  state is invariant with respect to CP-conjugation. Note that CP-conjugation changes the sign of  $A_{NS}$ , while  $A_{FB}$  is left unchanged. A non-zero  $A_{NS}$  would indicate CP-violation.

We study three data sets: (i)  $p\bar{p} \rightarrow \Lambda(\bar{\Lambda})X$ , (ii)  $p\bar{p} \rightarrow J/\psi\Lambda(\bar{\Lambda})X$ , and (iii)  $p\bar{p} \rightarrow \mu^\pm\Lambda(\bar{\Lambda})X$ , and the corresponding control samples with  $K_S$  instead of  $\Lambda$  or  $\bar{\Lambda}$ . Data set (i) is collected with a trigger on beam crossing (‘‘zero bias events’’) or with a trigger on energy deposited in forward counters (‘‘minimum bias events’’). Data set (ii) is selected with a suite of single muon, dimuon and dedicated  $J/\psi$  triggers, from which  $J/\psi \rightarrow \mu^+\mu^-$  candidates in association with a  $\Lambda$  or  $\bar{\Lambda}$  are reconstructed. Data set (iii) is selected with a suite of single muon triggers having a  $\mu$  and  $\Lambda$  in the final state. Data set (i) is unbiased, while most events in data sets (ii) and (iii) contain heavy quarks  $b$  or  $c$ . Data set (iii) has the same muon triggers and muon selections as in Refs. [4, 5]. The number of events in each data sample is summarized in Table I. There is no physical reason to require a  $J/\psi$  or  $\mu$ : data sets (ii) and (iii) are analyzed because they are well defined and available, and data set (iii) is huge.

TABLE I: Number of events in each data set with  $\Lambda$ ,  $\bar{\Lambda}$  or  $K_S$  with  $p_T > 2.0$  GeV.

Data set	Number of events	Data set	Number of events
$p\bar{p} \rightarrow \Lambda(\bar{\Lambda})X$	$5.85 \times 10^5$	$p\bar{p} \rightarrow K_S X$	$2.33 \times 10^6$
$p\bar{p} \rightarrow J/\psi \Lambda(\bar{\Lambda})X$	$2.50 \times 10^5$	$p\bar{p} \rightarrow J/\psi K_S X$	$6.55 \times 10^5$
$p\bar{p} \rightarrow \mu^\pm \Lambda(\bar{\Lambda})X$	$1.15 \times 10^7$	$p\bar{p} \rightarrow \mu^\pm K_S X$	$5.34 \times 10^7$

FIG. 1: Fit to the invariant mass histogram of  $\Lambda \rightarrow p\pi^-$  for  $0.1 < y < 1.0$ ,  $p_T > 2.0$  GeV, muon charge  $q = +1$ , solenoid magnet polarity  $\text{sol} = -1$ , and toroid magnet polarity  $\text{tor} = -1$ , for the  $p\bar{p} \rightarrow \mu\Lambda(\bar{\Lambda})X$  data.

## II. DETECTOR AND DATA

The DØ detector is described in [1–3]. The collision region is surrounded by a central-tracking system that comprises a silicon micro-strip vertex detector and a central fiber tracker, both located within a 1.9 T superconducting solenoidal magnet [1], surrounded successively by the liquid argon-uranium calorimeters, layer A of the muon system [2] (with drift chambers and scintillation trigger counters), the 1.8 T magnetized iron toroids, and two similar muon detector layers B and C after the toroids. The designs are optimized for vertex finding, tracking, and muon trigger and identification at pseudo-rapidities  $|\eta|$  less than 2.5, 3.0 and 2.1 respectively.

The solenoid and toroid magnet polarities were reversed about once every two weeks during data taking so that each of the four solenoid-toroid polarity combinations collected approximately the same number of events. All asymmetries are measured independently for each of the four solenoid-toroid polarity combinations, and then these asymmetries are averaged with equal weights.

The  $\Lambda$ 's,  $\bar{\Lambda}$ 's and  $K_S$ 's are reconstructed from pairs of oppositely charged tracks with a common vertex ( $V^0$ ). These tracks are required to have no more than four missing hits downstream of the vertex (per track), no more than two hits upstream of the vertex (summed over the two tracks), each track is required to have an impact parameter in the transverse plane (IP) with respect to the primary vertex with a significance of at least two standard deviations, and the  $V^0$  is required to have an IP significance less than three standard deviations. The distance in the transverse plane from the primary vertex to the  $V^0$  vertex is required to be greater than 4 mm. The  $V^0$  is required to have  $2.0 \text{ GeV} < p_T < 25 \text{ GeV}$  and pseudo-rapidity  $|\eta| < 2.2$ . For  $\Lambda$ 's and  $\bar{\Lambda}$ 's, the proton (pion) mass is assigned to the daughter track with larger (smaller) momentum. This assignment is nearly always correct because the decay  $\Lambda \rightarrow p\pi^-$  is barely above threshold. We require that the  $V^0$  daughter tracks be different from any muon track. Invariant mass histograms are fit with a double Gaussian (with free means, widths and normalizations) for the signal, and a second degree polynomial for the background. An example fit is presented in Fig. 1.

Control samples with  $K_S$  are analyzed exactly as the corresponding sets with  $\Lambda$  or  $\bar{\Lambda}$ , except that the track with larger momentum is assigned the pion mass, instead of the proton mass. Note that we count separately decays

$K_S \rightarrow \pi^+\pi^-$  and  $K_S \rightarrow \pi^-\pi^+$ , where the first pion has the larger total momentum. This way the former decay has kinematics similar to  $\Lambda$  decays, while the latter is similar to  $\bar{\Lambda}$  decays. The  $p\bar{p}$  collisions produce  $K^0$ 's and  $\bar{K}^0$ 's that we observe as resonances in invariant mass histograms of  $K_S \rightarrow \pi^+\pi^-$  decays. Since this final state does not distinguish the parents  $K^0$  from  $\bar{K}^0$  (neglecting CP violation),  $K_S$  decays do not distinguish the  $p$  and  $\bar{p}$  directions, have no physics asymmetries, and so constitute a control sample to study detector effects.

Antiprotons have a larger inelastic cross-section with the detector material than protons. This difference results in a higher detection efficiency for  $\Lambda$ 's than  $\bar{\Lambda}$ 's. This difference in efficiencies does not modify the asymmetries  $A'_{FB}$  or  $A'_{NS}$  (neglecting higher order terms in the asymmetries).

Another detector effect is of geometric origin (differences can occur as well from different electronic responses in the North and South halves of the DØ detector). Consider an event with  $\Lambda \rightarrow p\pi^-$ , and the charge-conjugate (C) event with  $\bar{\Lambda} \rightarrow \bar{p}\pi^+$ , with the same momenta for all corresponding tracks. Assume that, due to some detector geometric effect, the former event has a larger acceptance times efficiency than the latter event for a given solenoid and toroid polarity. Now reverse these polarities. The tracks of the event  $\Lambda \rightarrow p\pi^-$  with one solenoid and toroid polarity coincide with the tracks of the event  $\bar{\Lambda} \rightarrow \bar{p}\pi^+$  with the opposite polarities, and vice versa. So with reversed polarities it is now the event with  $\bar{\Lambda} \rightarrow \bar{p}\pi^+$  that has the larger acceptance times efficiency. The conjugation  $\Lambda \leftrightarrow \bar{\Lambda}$  reverses the sign of  $A'_{FB}$ , and leaves  $A'_{NS}$  unchanged. We conclude that by averaging over opposite solenoid and toroid polarities, geometrical detector effects are canceled for  $A'_{FB}$ , but not for  $A'_{NS}$  (neglecting higher order terms in the asymmetries, and if C symmetry holds).

We correct  $A'_{NS}$  using  $K_S$  by setting  $A_{NS} = A'_{NS} - A'_{NS}(K_S)$ , with an appropriate systematic uncertainty (discussed below). We correct  $A'_{FB}$  using  $K_S$  by setting  $A_{FB} = A'_{FB} - A'_{FB}(K_S)$ , with an appropriate systematic uncertainty (discussed below). Other observables that are corrected with measurements with  $K_S$  are  $\langle y(\Lambda) \rangle - \langle y(\bar{\Lambda}) \rangle$  and  $\langle p_z(\Lambda) \rangle - \langle p_z(\bar{\Lambda}) \rangle$ .

The systematic uncertainties of raw asymmetries are measured with the large control sample  $p\bar{p} \rightarrow \mu^\pm K_S X$  (in a few cases these uncertainties were increased as a result of cross-checks and studies of measurements with the three data sets). The systematic uncertainties of the corrections  $A'_{NS}(K_S)$  or  $A'_{FB}(K_S)$  are taken to be equal to 1/3 of these corrections. The systematic uncertainties of the raw asymmetries and of their corrections are added in quadrature. The factor 1/3 is estimated by comparing  $A'_{NS}$  for  $\Lambda/\bar{\Lambda}$  with  $A'_{NS}(K_S)$  for the different data sets,  $p_T$  cuts, and magnet polarities. (For example, compare measurements with  $\Lambda$  and  $K_S$  in the second column of Table II below: they are generally within 10% of each other, so the factor 1/3 is conservative.)

### III. ANALYSIS OF EVENTS $p\bar{p} \rightarrow \mu^\pm \Lambda(\bar{\Lambda}) X$

To study the asymmetries with a large data set, we consider  $p\bar{p} \rightarrow \mu^\pm \Lambda(\bar{\Lambda}) X$  events. The muon trigger and selection are the same as in [4, 5]. We assume that the rates for  $\mu^+$  and  $\mu^-$  are the same, except for muons from kaon decay which are significantly asymmetric because the  $K^+$  have a longer inelastic interaction length in the calorimeter than the  $K^-$ , and hence have more time to decay [4, 5].

Rapidity distributions for reconstructed  $\Lambda$ 's and  $\bar{\Lambda}$ 's are presented in Fig. 2. We find that there are more events  $\Lambda\mu^+$  and  $\bar{\Lambda}\mu^-$ , than events  $\Lambda\mu^-$  and  $\bar{\Lambda}\mu^+$ . Examples of decays with a  $\Lambda\mu^+$  correlation are:  $\Lambda_c^+ \rightarrow \Lambda\mu^+\nu_\mu$ , and  $p\bar{p} \rightarrow \Lambda K^+ X$  followed by  $K^+ \rightarrow \mu^+\nu_\mu$ . The reverse  $\Lambda\mu^-$  correlation occurs for  $\Lambda_b \rightarrow \mu^-\Lambda_c^+\bar{\nu}_\mu X$  with  $\Lambda_c^+ \rightarrow \Lambda X$ . Figure 3 presents the asymmetries  $A_{FB}$  for  $p_T$  of  $\Lambda$  or  $\bar{\Lambda}$  greater than 2.0, 4.0 or 6.0 GeV, for the sum of events with  $\mu^+$  and  $\mu^-$ .

For each muon charge  $q = \pm 1$ , each solenoid magnet polarity  $\text{sol} = \pm 1$ , and each toroid magnet polarity  $\text{tor} = \pm 1$  we obtain the counts  $N_F(\Lambda)$ ,  $N_B(\Lambda)$ ,  $N_F(\bar{\Lambda})$  and  $N_B(\bar{\Lambda})$  by fitting invariant mass histograms. We then obtain the asymmetries from Eqs. (2). The results are summarized in Table II for  $\Lambda$ 's and  $\bar{\Lambda}$ 's with  $0.1 < |y| < 2.2$  and  $p_T > 2.0$  GeV. Note that the asymmetries depend on  $q$ ,  $\text{sol}$  and  $\text{tor}$ . The asymmetries averaged over  $\text{sol}$  and  $\text{tor}$  are also presented in Table II. We define

$$\begin{aligned} A'_{FB1} &\equiv \frac{1}{2}(A'_{FB}(\mu^+) + A'_{FB}(\mu^-)), \\ A'_{FB2} &\equiv \frac{1}{2}(A'_{FB}(\mu^+) - A'_{FB}(\mu^-)). \end{aligned} \quad (3)$$

These asymmetries are summarized in Table III for  $\Lambda$  ( $\bar{\Lambda}$ ) and  $K_S$ . Averaging over opposite solenoid and toroid polarities cancels detector geometrical effects for  $A'_{FB1}$  and  $A'_{NS2}$ , but not for  $A'_{FB2}$  and  $A'_{NS1}$  (at first order in the asymmetries, and in the limits of C symmetry, and symmetry in the  $\mu^+$  and  $\mu^-$  from the  $K_S$  decay).

From Table III we observe the following:

1. The asymmetries  $A'_{NS1}(K_S)$  and  $A'_{NS2}(K_S)$  are significantly different from zero, and are comparable with the corresponding asymmetries for  $\Lambda$  ( $\bar{\Lambda}$ ).  $A'_{NS1}$  is dominated by detector geometric asymmetries, as expected. We

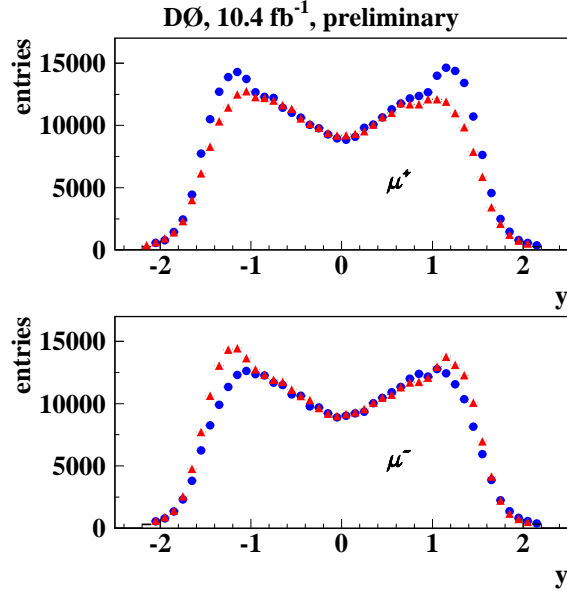


FIG. 2: Histograms of rapidity  $y$  of reconstructed  $\Lambda$ 's (circles) and  $\bar{\Lambda}$ 's (triangles) for events with a  $\mu^+$  (upper plot) or a  $\mu^-$  (lower plot), for  $p_T > 4.0$  GeV.

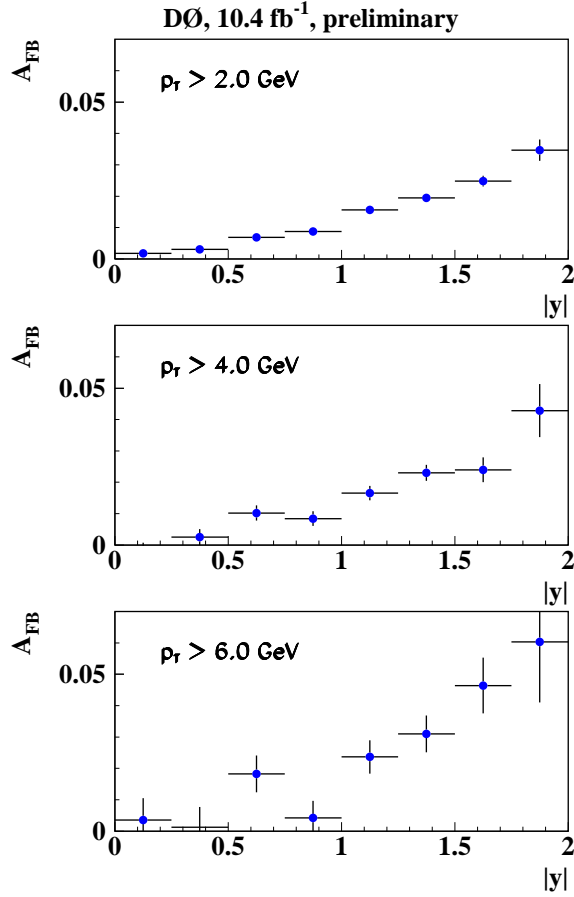


FIG. 3: Asymmetry  $A_{FB}$  as a function of  $|y|$  for events  $p\bar{p} \rightarrow \mu^\pm \Lambda(\bar{\Lambda}) X$  for  $p_T > 2.0$  GeV (upper plot),  $p_T > 4.0$  GeV, and  $p_T > 6.0$  GeV. Uncertainties are statistical. The systematic uncertainties are  $\pm 0.0006$ ,  $\pm 0.0010$  and  $\pm 0.0051$  respectively.

TABLE II: Asymmetries obtained for muon charge  $q$ , solenoid magnet polarity  $\text{sol}$ , and toroid magnet polarity  $\text{tor}$ , of  $\Lambda$ 's and  $\bar{\Lambda}$ 's with  $0.1 < |y| < 2.2$  and  $p_T > 2.0$  GeV. The averages of asymmetries are taken with equal weights. Uncertainties are statistical.

$q$	$\text{sol}$	$\text{tor}$	$A'_{FB} \times 100$	$A'_{NS} \times 100$
+1	-1	-1	$+0.822 \pm 0.123$	$+0.755 \pm 0.123$
+1	-1	+1	$+1.593 \pm 0.125$	$-0.025 \pm 0.125$
+1	+1	-1	$+0.999 \pm 0.126$	$+1.179 \pm 0.126$
+1	+1	+1	$+1.225 \pm 0.120$	$-0.093 \pm 0.120$
+1	average		$+1.160 \pm 0.062$	$+0.454 \pm 0.062$
-1	-1	-1	$+1.134 \pm 0.125$	$+0.059 \pm 0.125$
-1	-1	+1	$+1.482 \pm 0.126$	$+1.487 \pm 0.126$
-1	+1	-1	$+0.950 \pm 0.131$	$+0.220 \pm 0.131$
-1	+1	+1	$+1.215 \pm 0.127$	$+1.278 \pm 0.127$
-1	average		$+1.195 \pm 0.064$	$+0.761 \pm 0.064$

TABLE III: Raw asymmetries  $A'_{FB}(q) \equiv A'_{FB1} + qA'_{FB2}$  and  $A'_{NS}(q) \equiv A'_{NS1} + qA'_{NS2}$  of  $\Lambda$ 's and  $K_S$ 's with  $0.1 < |y| < 2.2$ . Uncertainties are statistical.

$A'_{FB1} \times 100$	$A'_{NS1} \times 100$
$A'_{FB2} \times 100$	$A'_{NS2} \times 100$
$\Lambda$ and $\bar{\Lambda}, p_T > 2.0$ GeV	
$+1.177 \pm 0.044$	$+0.607 \pm 0.044$
$-0.018 \pm 0.044$	$-0.153 \pm 0.044$
$\Lambda$ and $\bar{\Lambda}, p_T > 4.0$ GeV	
$+1.424 \pm 0.183$	$+0.915 \pm 0.183$
$+0.109 \pm 0.183$	$-0.376 \pm 0.183$
$\Lambda$ and $\bar{\Lambda}, p_T > 6.0$ GeV	
$+1.649 \pm 0.510$	$+1.722 \pm 0.510$
$+0.089 \pm 0.510$	$-0.535 \pm 0.510$
$K_S, p_T > 2.0$ GeV	
$+0.032 \pm 0.015$	$+0.665 \pm 0.015$
$-0.032 \pm 0.015$	$-0.149 \pm 0.015$
$K_S, p_T > 4.0$ GeV	
$-0.059 \pm 0.027$	$+0.807 \pm 0.027$
$-0.043 \pm 0.027$	$-0.268 \pm 0.027$
$K_S, p_T > 6.0$ GeV	
$+0.274 \pm 0.085$	$+1.002 \pm 0.085$
$-0.113 \pm 0.085$	$-0.191 \pm 0.085$

note that  $A'_{NS2} - A'_{NS2}(K_S)$  is consistent with zero. Therefore we take  $A_{NS} = A'_{NS1} - A'_{NS1}(K_S)$ , and assign  $A'_{NS1}(K_S)/3$  as the systematic uncertainty. The factor 1/3 is conservative as can be seen in the second column of Table III.

2. The asymmetries  $A'_{FB2}$  for  $\Lambda(\bar{\Lambda})$  or  $K_S$ , are consistent with zero, so we take  $A_{FB} = A'_{FB1} - A'_{FB1}(K_S)$ , and assign  $A'_{FB1}(K_S)/3$  as the systematic uncertainty of this correction, and estimate a systematic uncertainty of  $A'_{FB1}$  from the measurements of  $A'_{FB1}$  and  $A'_{FB2}$  for  $K_S$  in Table III. These two systematic uncertainties are added in quadrature.

The observations that  $A'_{NS2} - A'_{NS2}(K_S)$  and  $A'_{FB2} - A'_{FB2}(K_S)$  are consistent with zero validates the measurements of  $A_{NS}$  and  $A_{FB}$  in spite of the  $\Lambda\mu$  correlations.

The asymmetries in Tables II and III are obtained from fits to invariant mass histograms. The asymmetries presented in Fig. 3 are obtained by counting  $\Lambda$  and  $\bar{\Lambda}$  candidates in a signal region, and subtracting the corresponding counts in two sideband regions. This method is adopted due to the large computational load of fitting the samples at all values of  $|y|$ .

For events  $p\bar{p} \rightarrow \mu^\pm \Lambda(\bar{\Lambda})X$  with  $0.1 < |y| < 2.2$  we obtain for  $\Lambda$  or  $\bar{\Lambda}$  with  $p_T > 2.0$  GeV:

$$\begin{aligned} A_{FB} &= 0.0115 \pm 0.0005 \text{ (stat)} \pm 0.0006 \text{ (syst)}, \\ \langle p_z(\Lambda) \rangle - \langle p_z(\bar{\Lambda}) \rangle &= 0.1149 \pm 0.0013 \text{ (stat)} \pm 0.0022 \text{ (syst)} \text{ GeV}, \\ \langle y(\Lambda) \rangle - \langle y(\bar{\Lambda}) \rangle &= 0.0236 \pm 0.0003 \text{ (stat)} \pm 0.0006 \text{ (syst)}. \end{aligned} \quad (4)$$

For  $\Lambda$  or  $\bar{\Lambda}$  with  $p_T > 4.0$  GeV:

$$\begin{aligned} A_{FB} &= 0.0148 \pm 0.0019 \text{ (stat)} \pm 0.0010 \text{ (syst)}, \\ \langle p_z(\Lambda) \rangle - \langle p_z(\bar{\Lambda}) \rangle &= 0.250 \pm 0.011 \text{ (stat)} \pm 0.005 \text{ (syst)} \text{ GeV}, \\ \langle y(\Lambda) \rangle - \langle y(\bar{\Lambda}) \rangle &= 0.0305 \pm 0.0013 \text{ (stat)} \pm 0.0010 \text{ (syst)}. \end{aligned} \quad (5)$$

For  $\Lambda$  or  $\bar{\Lambda}$  with  $p_T > 6.0$  GeV:

$$\begin{aligned} A_{FB} &= 0.0137 \pm 0.0052 \text{ (stat)} \pm 0.0051 \text{ (syst)}, \\ \langle p_z(\Lambda) \rangle - \langle p_z(\bar{\Lambda}) \rangle &= 0.552 \pm 0.045 \text{ (stat)} \pm 0.015 \text{ (syst)} \text{ GeV}, \\ \langle y(\Lambda) \rangle - \langle y(\bar{\Lambda}) \rangle &= 0.0488 \pm 0.0035 \text{ (stat)} \pm 0.0026 \text{ (syst)}. \end{aligned} \quad (6)$$

The asymmetry  $A_{NS}$  for  $p_T > 2.0$  GeV and  $0.1 < |y| < 2.2$  is

$$A_{NS} = -0.0006 \pm 0.0005 \text{ (stat)} \pm 0.0023 \text{ (syst)}. \quad (7)$$

We note that  $A_{NS}$  is consistent with zero so we observe no CP violation, while  $A_{FB}$  is small, but significantly different from zero.

#### IV. ANALYSIS OF MINIMUM BIAS EVENTS $p\bar{p} \rightarrow \Lambda(\bar{\Lambda})X$

Histograms of  $p_T$ ,  $p_z$  and  $y$  of reconstructed  $\Lambda$ 's and  $\bar{\Lambda}$ 's are shown in Fig. 4. The corresponding asymmetries  $A_{FB}$  are presented in Fig. 5. The raw asymmetries for  $p_T > 2.0$  GeV and  $0.1 < |y| < 2.2$  for  $\Lambda$  and  $\bar{\Lambda}$  are measured to be

$$A'_{FB} = 0.0112 \pm 0.0018, \text{ and} \quad (8)$$

$$A'_{NS} = 0.0000 \pm 0.0018. \quad (9)$$

For  $K_S$ :

$$A'_{FB} = 0.0010 \pm 0.0008, \text{ and} \quad (10)$$

$$A'_{NS} = +0.0012 \pm 0.0008. \quad (11)$$

For minimum bias events  $p\bar{p} \rightarrow \Lambda(\bar{\Lambda})X$ , and  $0.1 < |y| < 2.2$ , we obtain for  $\Lambda$  or  $\bar{\Lambda}$  with  $p_T > 2.0$  GeV:

$$\begin{aligned} A_{FB} &= 0.0102 \pm 0.0020 \text{ (stat)} \pm 0.0008 \text{ (syst)}, \\ A_{NS} &= -0.0013 \pm 0.0020 \text{ (stat)} \pm 0.0010 \text{ (syst)}, \\ \langle p_z(\Lambda) \rangle - \langle p_z(\bar{\Lambda}) \rangle &= 0.1011 \pm 0.0057 \text{ (stat)} \pm 0.0022 \text{ (syst)} \text{ GeV}, \\ \langle y(\Lambda) \rangle - \langle y(\bar{\Lambda}) \rangle &= 0.0234 \pm 0.0013 \text{ (stat)} \pm 0.0006 \text{ (syst)}. \end{aligned} \quad (12)$$

The asymmetry  $A_{FB}$  shown in Fig. 5 is compared, in Fig. 6, with other experiments that study collisions  $pZ \rightarrow \Lambda(\bar{\Lambda})X$  for several targets  $Z$ . For the  $D\bar{O}$  minimum bias data in Fig. 6 we plot  $(\sigma_B(\Lambda) + \sigma_B(\bar{\Lambda})) / (\sigma_F(\Lambda) + \sigma_F(\bar{\Lambda})) = (1 - A_{FB}) / (1 + A_{FB})$ . From Fig. 6 we conclude that the  $\bar{\Lambda}/\Lambda$  production ratio for  $p_z > 0$  is approximately a universal function (within the uncertainties) of the ‘‘rapidity loss’’  $\Delta y \equiv y_p - y$ , independent of  $\sqrt{s}$  or target  $Z$ . Here  $y_p$  is the rapidity of the proton beam, and  $y$  is the rapidity of the  $\Lambda$  or  $\bar{\Lambda}$ .

#### V. ANALYSIS OF EVENTS $p\bar{p} \rightarrow J/\psi \Lambda(\bar{\Lambda})X$

The raw asymmetries for  $p_T > 2.0$  GeV and  $0.1 < |y| < 2.2$  are measured to be

$$A'_{FB} = 0.0149 \pm 0.0038, \text{ and} \quad (13)$$

$$A'_{NS} = 0.0058 \pm 0.0038, \quad (14)$$

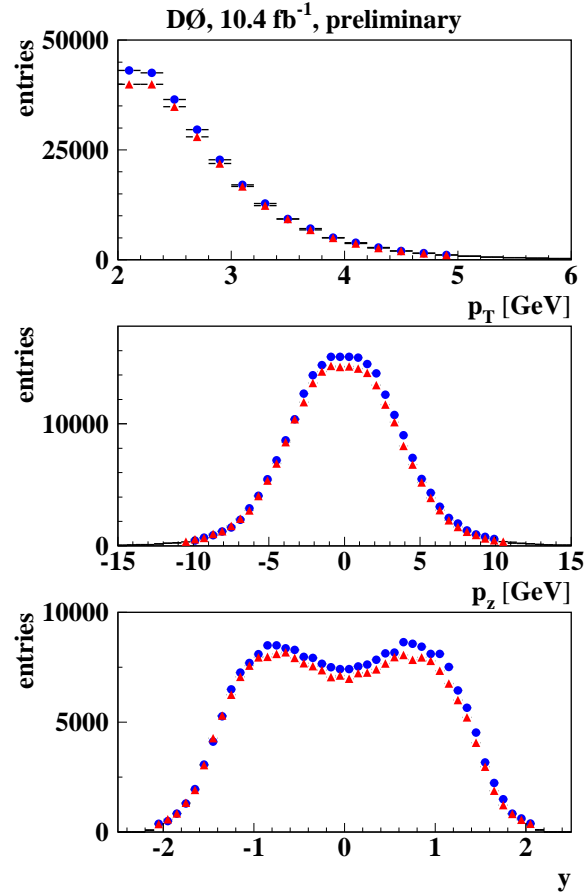


FIG. 4: Histograms of  $p_T$  (upper plot),  $p_z$  and  $y$  of reconstructed  $\Lambda$ 's (circles) and  $\bar{\Lambda}$ 's (triangles) with  $p_T > 2.0$  GeV, for the minimum bias data sample  $p\bar{p} \rightarrow \Lambda(\bar{\Lambda})X$ .

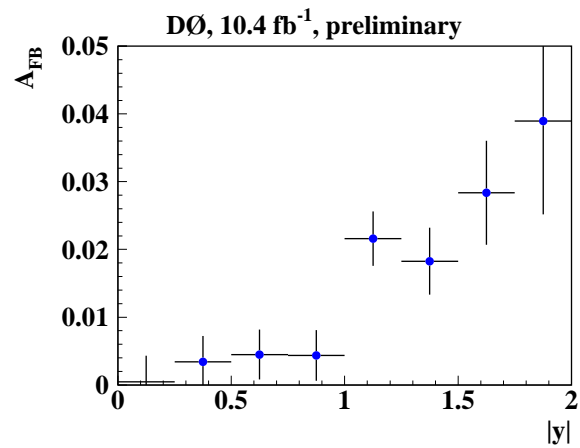


FIG. 5: Asymmetry  $A_{FB}$  of reconstructed  $\Lambda$ ,  $\bar{\Lambda}$  with  $p_T > 2.0$  GeV, as a function of  $|y|$ , for the minimum bias data sample  $p\bar{p} \rightarrow \Lambda(\bar{\Lambda})X$ . Uncertainties are statistical. The systematic uncertainty of  $A_{FB}$  is  $\pm 0.0008$ .

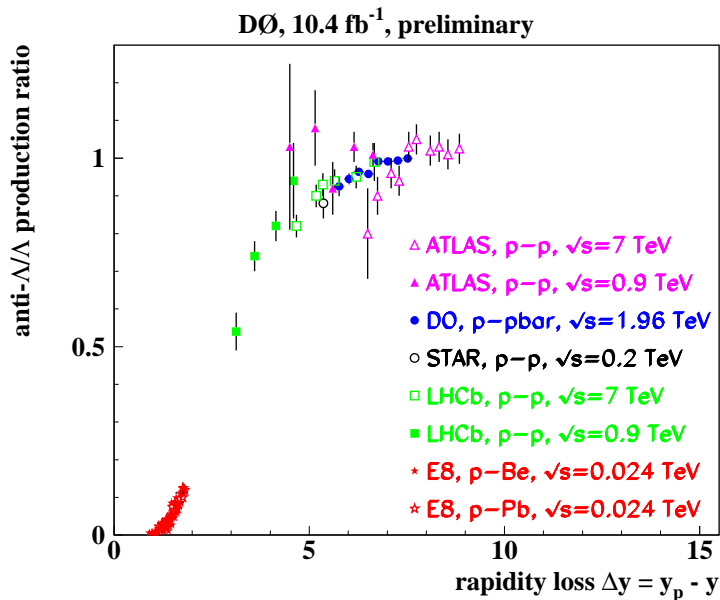


FIG. 6:  $\bar{\Lambda}/\Lambda$  production ratio as a function of the rapidity loss  $\Delta y \equiv y_p - y$  for several experiments (over 37 years!) that study reactions  $pZ \rightarrow \Lambda(\bar{\Lambda})X$ . The experiments are ATLAS [6], DØ(this analysis), STAR [7], LHCb [8], and the fixed target experiment Fermilab E8 studying 300 GeV  $p$ -Be and  $p$ -Pb collisions [9].

for  $\Lambda$  and  $\bar{\Lambda}$ 's, and

$$A'_{FB} = 0.0021 \pm 0.0024, \text{ and} \quad (15)$$

$$A'_{NS} = 0.0045 \pm 0.0024 \quad (16)$$

for  $K_S$ 's. The asymmetries  $A_{FB}$  and  $A'_{NS}$  are presented in Fig. 7. For events  $p\bar{p} \rightarrow J/\psi\Lambda(\bar{\Lambda})X$ , and  $0.1 < |y| < 2.2$ , we obtain for  $\Lambda$  or  $\bar{\Lambda}$  with  $p_T > 2.0$  GeV:

$$\begin{aligned} A_{FB} &= 0.0128 \pm 0.0045 \text{ (stat)} \pm 0.0016 \text{ (syst)}, \\ A_{NS} &= 0.0013 \pm 0.0045 \text{ (stat)} \pm 0.0024 \text{ (syst)}, \\ \langle p_z(\Lambda) \rangle - \langle p_z(\bar{\Lambda}) \rangle &= 0.092 \pm 0.011 \text{ (stat)} \pm 0.002 \text{ (syst)} \text{ GeV}, \\ \langle y(\Lambda) \rangle - \langle y(\bar{\Lambda}) \rangle &= 0.0224 \pm 0.0027 \text{ (stat)} \pm 0.0006 \text{ (syst)}. \end{aligned} \quad (17)$$

Note that the results for the three data sets  $p\bar{p} \rightarrow \Lambda(\bar{\Lambda})X$ ,  $p\bar{p} \rightarrow J/\psi\Lambda(\bar{\Lambda})X$  and  $p\bar{p} \rightarrow \mu^\pm\Lambda(\bar{\Lambda})X$  are in agreement within uncertainties, in spite of their different sample composition. A comparison is presented in Fig. 8.

## VI. CONCLUSIONS

We have measured the forward-backward asymmetry of  $\Lambda$ ,  $\bar{\Lambda}$  production  $A_{FB}$ , and the related asymmetries  $\langle y(\Lambda) \rangle - \langle y(\bar{\Lambda}) \rangle$  and  $\langle p_z(\Lambda) \rangle - \langle p_z(\bar{\Lambda}) \rangle$ , of three data sets:  $p\bar{p} \rightarrow \Lambda(\bar{\Lambda})X$ ,  $p\bar{p} \rightarrow J/\psi\Lambda(\bar{\Lambda})X$ , and  $p\bar{p} \rightarrow \mu^\pm\Lambda(\bar{\Lambda})X$ . The asymmetry  $A_{FB}$  is significantly different from zero. The  $\bar{\Lambda}/\Lambda$  production ratio is approximately a universal function (within the uncertainties) of the proton ‘‘rapidity loss’’  $y_p - y$ , and does not depend significantly (or depends only weakly) on the total center of mass energy  $\sqrt{s}$  or target (see Fig. 6), or the data set or data composition (see Fig. 8), or  $p_T$  (see Fig. 3). These observations suggest that a  $u$ -quark of some protons becomes replaced by an  $s$  quark in the collision, resulting in a  $\Lambda$  with loss of rapidity. The measurement of  $A_{NS}$  is consistent with zero to within 0.23%, see Eqs. (12), (17) and (7), so we observe no significant CP violation.

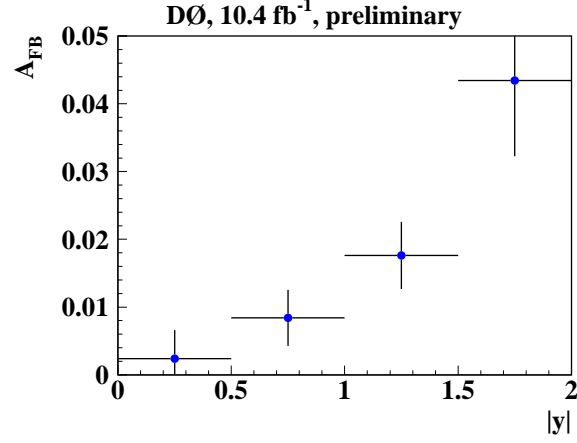


FIG. 7: Asymmetry  $A_{FB}$  of reconstructed  $\Lambda$ ,  $\bar{\Lambda}$  with  $p_T > 2.0$  GeV, as a function of  $|y|$ , for the data sample  $p\bar{p} \rightarrow J/\psi\Lambda(\bar{\Lambda})X$ . Uncertainties are statistical. The systematic uncertainty of  $A_{FB}$  is  $\pm 0.0016$ .

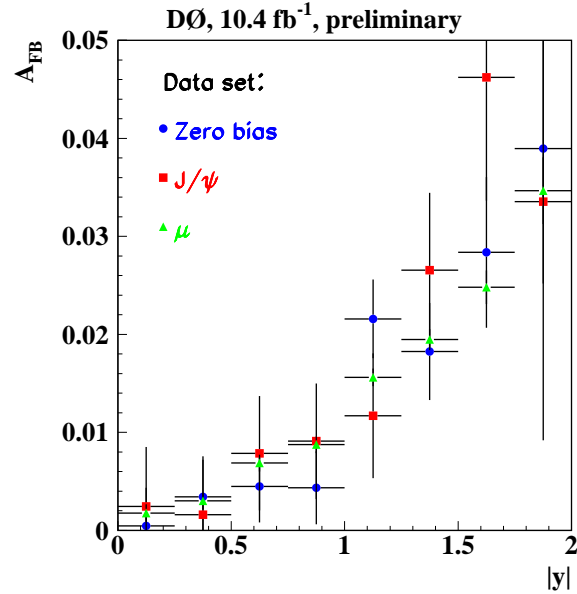


FIG. 8: Asymmetry  $A_{FB}$  as a function of  $|y|$  for events  $p\bar{p} \rightarrow \Lambda(\bar{\Lambda})X$  (circles),  $p\bar{p} \rightarrow J/\psi\Lambda(\bar{\Lambda})X$  (squares), and  $p\bar{p} \rightarrow \mu^\pm\Lambda(\bar{\Lambda})X$  (triangles) for  $p_T > 2.0$  GeV. Uncertainties are statistical. The systematic uncertainties are  $\pm 0.0008$ ,  $\pm 0.0016$  and  $\pm 0.0006$  respectively.

### Acknowledgments

We thank the staffs at Fermilab and collaborating institutions, and acknowledge support from the Department of Energy and National Science Foundation (United States of America); Alternative Energies and Atomic Energy Commission and National Center for Scientific Research/National Institute of Nuclear and Particle Physics (France); Ministry of Education and Science of the Russian Federation, National Research Center “Kurchatov Institute” of the Russian Federation, and Russian Foundation for Basic Research (Russia); National Council for the Development of Science and Technology and Carlos Chagas Filho Foundation for the Support of Research in the State of Rio de Janeiro (Brazil); Department of Atomic Energy and Department of Science and Technology (India); Administrative Department of Science, Technology and Innovation (Colombia); National Council of Science and Technology (Mexico); National Research Foundation of Korea (Korea); Foundation for Fundamental Research on Matter (The Netherlands); Science and Technology Facilities Council and The Royal Society (United Kingdom); Ministry of Education, Youth

and Sports (Czech Republic); Bundesministerium für Bildung und Forschung (Federal Ministry of Education and Research) and Deutsche Forschungsgemeinschaft (German Research Foundation) (Germany); Science Foundation Ireland (Ireland); Swedish Research Council (Sweden); China Academy of Sciences and National Natural Science Foundation of China (China); and Ministry of Education and Science of Ukraine (Ukraine).

---

- [1] V.M. Abazov *et al.* (D0 Collaboration), Nucl. Instrum. Methods in Phys. Res. A **565**, 463 (2006).
- [2] V.M. Abazov *et al.*, Nucl. Instrum. Methods in Phys. Res. A **552**, 372 (2005).
- [3] S.N. Ahmed *et al.*, (D0 Collaboration), Nucl. Instrum. Methods Phys. Res. A **634**, 8 (2011); R. Angstadt *et al.*, (D0 Collaboration), Nucl. Instrum. Methods Phys. Res. A **622**, 298 (2010); V.M. Abazov *et al.* (D0 Collaboration), Nucl. Instrum. Methods in Phys. Res. Sect. A **737**, 281 (2014).
- [4] V.M. Abazov *et al.* (D0 Collaboration), Phys. Rev. D **89** 012002 (2014).
- [5] V.M. Abazov *et al.* (D0 Collaboration), Phys. Rev. D **84**, 052007 (2011).
- [6] G. Aad *et al.* (ATLAS Collaboration), Phys. Rev. D **85** (2012) 012001.
- [7] B.I. Abelev *et al.* (STAR Collaboration), Phys. Rev. C **75**, 064901 (2007).
- [8] R. Aaij *et al.* (LHCb Collaboration), J. High Energy Phys. 1108 (2011) 034.
- [9] P. Skubic *et al.* (E8 Collaboration), Phys. Rev. D **18**, 3115 (1978).